Journal of Engineering Science and Technology
Vol. 12, No. 10 (2017) 2613 - 2627

QUASI-STATIC FIELD ANALYSIS OF PERMANENT MAGNET GENERATOR USING H-HIERARCHICAL ADAPTIVE FINITE ELEMENT METHOD

CHETAN VASUDEVA[1,2,*], SANJAY MARWAHA[1]

[1]Department of Electrical & Instrumentation Engineering,
S.L.I.E.T, Longowal-148106, Punjab, India
[2]Department of Electrical Engineering, D.A.V. University, Jalandhar-144012, Punjab, India
*Corresponding Author: chetan.vasudeva@gmail.com

Abstract

Researchers have always shown keen interest in predetermining the electromagnetic field behavior inside an electrical machine at the design stage. Material properties of permanent magnet, selection of optimum air gap during the electromagnetic, thermal and structural design of generator are considered to be vital factors for an ideal machine. Generator output, heat rise, weight, and cost are a few of the characteristics which are directly influenced by the selection of the most advantageous material properties. Moreover, most theoretical studies have been conducted assuming that the air gap flux is sinusoidally distributed. The actual conduct of the air gap flux with the length of air gap and its impression on the performance of the generator has not been analyzed so far. In this paper, field analysis of permanent magnet generator using finite element method has been carried out to show the best material properties and air gap for optimum pattern.

Keywords: Finite element method, Field analysis, Permanent magnet generator, Hybrid mesh, Air gap.

1. Introduction

Latest machines must be compact, light, and torque dense, which are often understood to survive extreme environmental and loading conditions. A permanent magnet machine has acquired recognition in late years. For electrical designs, not only accuracy of calculation but also appropriate determination of configurations of stator and rotor cores to meet the exact machine specification is required [1]. Knowledge of the air flow in a machine is crucial for design purposes,

Nomenclatures

A_z	z component of magnetic vector potential
A	Total area of cross-section, m^2
a	Area under element
C	Boundary
F	Forcing function
H_θ	Tangential component of magnetic field intensity
$h_1 h_2 h_3$	Side lengths of triangle
J	Current density
L	Length of generator in three dimensions, m
N	Shape function
N_s	Number of nodes on the air gap boundaries
$\hat{n}$	Unit outward vector normal to the boundary
NN	Number of turns of winding
R	Boundary integral term
S	System matrix
T_c	Cogging torque, Nm
v	Magnetic reluctivity
W_g	Stored magnetic energy

Greek Symbols

α	Rotor angle
∇	Divergence operator
$\iint_\Omega$	Second integral
$\oint_C$	Surface integral
μ	Permeability
σ	Electrical conductivity
ρ	Density
$curl$	Curl operator
$\sum_{winding}$	Summation over all winding cross-section

Abbreviations

ALE	Arbitrary Lagrangian-Eulerian
FEM	Finite Element Method
NdFeB	Neodymium Iron Boron
PM	Permanent Magnet
RPM	Revolution Per Minute
SmCo	Samarium Cobalt

particularly where air gap limits the heat transfer [2].

The electromagnetic forces exerted in the rotating generator cause serious troubles if the selection of the proper air gap and the magnetic material is not made.

Detailed analysis of the field in the air gap of a permanent magnet generator is of great importance for precise prediction of the performance. Calculation of the magnetic field in the air gap with slotted stators due to the stator current has been documented in the literature by Polinder and Hoeijmaker [3]. The main parameters such as electromagnetic torque, magnetic radial forces, and flux-linkages can be evaluated directly from magnetic field distribution in the air gap. Particularly, the flux through the magnet must be defined as tangential or normal to the magnetization direction [4]. Precise field calculations in generator could be carried out using h-hierarchal adaptive finite element method. The tool is well accepted and more flexible for the predicting accurate performance. The modeling of electrical machines frequently requires that the virtual movement between stator and rotor should be brought into account. In the previous years, a number of methods and techniques have been established to tackle the movement without re-meshing the analyses domain, such as the air gap element, moving layer method and the Lagrangian multipliers-interpolation method [5]. Using conventional methods the solution of electromagnetic field inside is based mostly on the solution of Maxwell's differential equations for magnetic and electric regions in the electric machines, which may be represented in an integral form [6]. On the other hand, unbalanced magnetic forces of electrical generator were analyzed using Fourier series and vibrations of these machines were predicted [7 - 10].

Electromagnetic characteristics of a double-stator radial-flux PM generator are studied using finite element analysis [11]. Static and quasi-static magnetic fields from given surface and volume distributions of electric current can be modeled using equivalent distributions of assumed magnetic charge and assumed magnetization. Magnetic charge model for a given line and surface along with volume distributions of electric current have been used for formulating numerous magnetic field problems [6].

The finite element method allows precise determination of machine parameters through magnetic field solutions. Using the finite element method, the domain is discretized into finite elements and field equation is applied to them. As numerous elements would be there, the time required for solution has to be more in duration.

In this paper the quasi static behavior of permanent magnet generator is analyzed when the machine undergoes mechanical and electromagnetic interactions. The finite element analysis tool is used to carry out the analysis for choosing the best permanent magnet material and the length of the air gap as an aid to optimize design parameters of the generator.

2. Permanent magnet generator

The permanent magnet generator is the most basic form of electrical machines. It's remarkable to note that permanent magnet machine doesn't require slip rings and brushes as they already have brushless excitation. Permanent magnets have replaced the rotor winding and reduced the rotor excitation loss; 20-30% of these losses are done away with [12]. The permanent magnet generator ensures a high reliability due to lack of brushes [13]. Eliminated loss results in bringing down the rise of generator temperature for which smaller and simpler cooling system can be put in. The reliability of the generator is increased with reduced effective temperatures. PM generator have advantages such as reduced size, lower installation and maintenance cost [14].

Table 1. Design specifications of analysis model.

Name	Value
Length of generator	0.4 m
Number of poles	16
Area of wire in stator	0.01257 m^2
Number of revolutions	60 RPM
Air gap	10 mm, 15 mm, 20 mm, 25 mm, 30 mm
Permanent magnet material	Alnico5, Alnico9, NdFe30, SmCo24, SmCo28

Permanent magnet machines are comparable to conventional synchronous or dc commutator machines. Armature windings and magnetic circuit can be identical in PM machines to those of conventional machines [15]. There is no similarity between PM machines and singly excited machines and these are frequently equated with machines such as induction motor or hysteresis machines. These machines have simple structure and are competitive in terms of cost, ease of assembly, size and volume. PM machines can be constructed in many nonstandard sizes and shapes, which normally compensate for cost penalty, especially for certain special applications. Permanent magnet materials such as Alnico, Samarium Cobalt, Neodymium, etc., are used for the modeling of the solid rotor. The rotor of the machine is made of nonmagnetic single shaft. The permanent magnet machine rotor is intended for maximum electromagnetic output. It is required that the generator should be compact and light so that it could be installed according to the need [16]. The modeling of the generator is such that the magnetic flux is maximized for a rotor, and at the same time it confirms that demagnetization is almost not possible. Structure of the rotor consists of annealed medium carbon steel with a potential of high permeability. In this paper the rotary motion of a rotor with permanent magnet induces voltage in the stator winding as shown in Fig. 1. The model is analyzed for the influence of generated voltage from material properties and air gap. The design is especially appropriate to utilize non rare earth magnets. The high coercive force can be applied to avoid the demagnetization on the exclusion of the rotor. The machine uses the stator with distributed winding. Permanent magnet generator offers high efficiency in operation; a simple and robust structure in construction because no field current and windings are inbuilt [16].

2.1. Length of air gap

Modeling in the air gap of rotating machine is complex. The length of air gap may be quite a few orders of magnitude smaller than the circumference. So, length of air gap in broad-spectrum deprives aspect ratio. Since, many layers of elements may be needed to attain a superior field solution, the elements in the air gap become vague during the computation. The length of the air gap magnetic field depends on permanent magnet and stator magneto motive force. Referable to the open slot configuration and magnetic saturation, the calculation of length of the air gap field becomes an intricate problem. For the permanent magnet rotors, the magnetic saturation may be ignored unless very high load current is tolerable, in large torque density design. The consequence of slot opening on the air gap field when the length of the air gap is reduced. As far as mechanical constraints allow the magnetic flux density increases, induced voltage increases and if the length of

the air gap is increased, the magnetic flux density and induced voltage decreases. Further, the variation of the air gap also affects power factor, magnetizing current, cooling noise, etc.

The air gap is a non-conducting domain and is aptly described by Poisson's equation. For two dimensional problem

$$\partial/\partial x = 0 \tag{1}$$

$$\nabla \times v\nabla \times A = J \tag{2}$$

Galerkin's approach applied to above equation yields

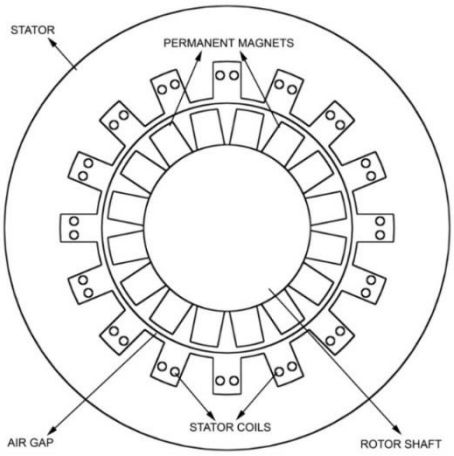

Fig. 1. Geometry for permanent magnet generator for 20 mm air gap.

$$\iint_\Omega v\left[\frac{\partial N}{\partial x}\frac{\partial A}{\partial x}+\frac{\partial N}{\partial y}\frac{\partial A}{\partial y}\right]dx\,dy-\iint_\Omega JN\,dx\,dy-\oint_c vN\frac{\partial A}{\partial \hat{n}}\,dC=0 \tag{3}$$

The set of boundary integral to zero, thereby yielding the homogeneous Neumann boundary condition is inherent in the configuration. The procedure implied uses the boundary integral term to the finite element equation, to the stationary and rotational domain to the solution in the air gap. The resulting system is represented in matrix form as

$$\begin{pmatrix}S_{11} & S_{12}\\ S_{21} & S_{22}\end{pmatrix}\begin{Bmatrix}A_1\\ A_2\end{Bmatrix}+\begin{Bmatrix}0\\ R\end{Bmatrix}=\begin{Bmatrix}F_1\\ F_2\end{Bmatrix} \tag{4}$$

Where R,

$$R=\{R_1,R_2,\dots\dots\dots,R_{N_B}\} \tag{5}$$

R_j is given by,

$$R_j=\oint_c -N_jH_\theta\,dC \tag{6}$$

Hence, in the air gap

$$\mu_o H=\nabla\times A \tag{7}$$

Therefore, in two dimensions

$$-\mu_o H_\theta=\frac{\partial A}{\partial r} \tag{8}$$

2.2. Permanent magnet

In the modern era permanent magnet machines have shown their existence partly due to the need for inexpensive and reliable excitation system. Permanent magnets, at present, are available with a wide range of characteristics, allowing a larger scope in the selection of magnet composition [17]. A high-quality permanent magnet is necessary to have a high coercive field intensity and high remanent induction. The high coercive field intensity is vital as it does not permit the magnet to be demagnetized and high remanent induction is usually related to the ability of magnet to induce high magnetic fields in magnetic circuits in which they are installed.

Permanent magnets can be classified as non-rare-earth type and rare earth type phenomena. Non-rare-earth magnets include Alnico (aluminum–nickel–cobalt) and ceramics (strontium and barium ferrites), non-rare-earth magnets are used in the many applications due to their low cost. Rare earth permanent magnets are unique as they can be considered as large maximum energy product. The maximum energy product (J/m^3) is the maximum value for the product of magnetizing force and induction, and is an indication of the strength of the material. A number of rare earth permanent magnet materials have been developed, including SmCo (samarium-cobalt) and NdFeB (neodymium–iron–boron) magnets. NdFeB material has a magnetizing force more than 10 times stronger than a traditional ferrite magnet, and its maximum energy product can easily reach 250 kJ/m^3. In early 80s, NdFeB emerged as an important class of high energy permanent magnet [18]. Information on some other magnets is also discussed by Moskowitz [19]. However, the magnetic performance of NdFeB material will depreciate quickly above about 180ºC. The corrosion and oxidation of NdFeB is comparatively high. Permanent magnet machines, particularly rare earth magnet machines are more advantageous compared to traditionally excited machines. Permanent magnet machines are also simple. The improvement of permanent magnets with elevated energy density has led to a bigger concern in the use of permanent magnets. Each material has its own pros and cons. A balance between cost and performance must be taken into account. The permanent magnet generator can be considered as a synchronous machine where the magnetizing coil is replaced by a permanent magnet. The coercive field intensity of magnetic materials is less than 20,000 A/m which are quite low. The material such as Alnico, Ferrite, Samarium cobalt and Neodymium iron boron having the value of coercive field intensity larger than 50,000 A/m are used in many applications. Table 2 shows the material specifications of permanent magnets.

Table 2. Specifications of magnetic material.

Material	B_r (T)	H_c (A/m)	μ_r
Alnico5	1.27	50929	2.49
Alnico9	1.05	119366	1.00
NdFe30	1.10	837999	1.03
SmCo24	1.01	756000	1.05
SmCo28	1.07	82000	1.04

Revolution in high energy permanent magnet persists with the aim of improving their static and dynamic response and escalating their energy density. Most permanent magnets follow differential permeability, i.e., $\tan\theta = B/H$ quite close to that of air (μ_r=1). Operating at P_1 point is the best choice as at this point the magnet

preserves its remanent induction nearer to maximum at B_0. If the operation point is further decided to be point P_2 it loses the remanent induction to a new value B_{02}. This results in the decline of performance below the permissible limits. Further, if it is operated at point P_3 the remanent induction loses its previous value and becomes zero. It is necessary to prevent operating below point P_1 as shown in Fig. 2.

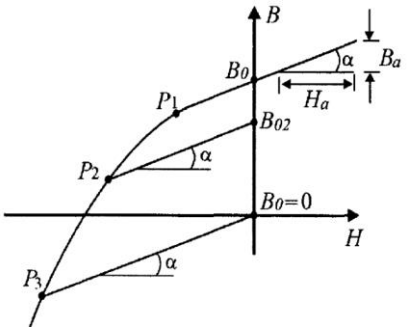

Fig. 2. Permanent magnet *B*-*H* curve.

Analysis using finite element method is basically founded on the subdivision of the whole sub domains. The essential depiction of an electromagnetic field is in terms of the electric field E and magnetic vector *H*. These vectors analyze the power of an electric field to do work on the charged body in translational motion and the power of magnetic field to execute work on a magnetic dipole in rotation respectively. The term *E* and *H* are closely associated with the electric displacement field (*D*) and magnetic field densities (*B*). The equations are interpreted as differential form of Maxwell's Equations.

$$curl\ E = -\partial B/\partial t \tag{9}$$

$$curl\ H = J + \partial D/\partial t \tag{10}$$

$$div\ D = \rho \tag{11}$$

$$div\ B = 0 \tag{12}$$

The FEM based analysis can be divided into the following steps [20]:

- Physical problem description.
- Problem definition and abstraction of physical problem.
- Pre-processing with the division into finite element, i.e., meshing, applications of loads and constraints.
- Solution passes with the formation of element equations and solution of element matrix.
- Post-processing pass with calculation of results.

The generator design is an exact time dependent model where the activity of the magnetic sources in the rotor is accounted for the boundary condition between stator and rotor. There is no Lorentz term in the equation, resulting in partial differential equation.

$$\sigma\frac{\partial A}{\partial t} + \nabla \times \left(\frac{1}{\mu}\nabla \times A\right) = 0 \tag{13}$$

The magnetic vector potential has only *z* component.

The rotary motion is modeled using moving mesh (ALE) application mode, in which the center part of the geometry, containing the rotor and part of the air gap, rotates with rotation transformation relative to the coordinate system of the stator. The minimum mesh element quality factor for 20 mm air gap generator model is around 0.7. Larger number of elements are required to calculate the field with sufficient precision [21].

Mesh Quality is denoted as

$$q = \frac{4\sqrt{3}a}{h_1^2+h_2^2+h_3^2} \tag{14}$$

The deformed meshes in the air gap have 4 layers and each layer takes in 396 elements and total of 1584 unknown elements in the 20 mm air gap. The number of unknown elements in the air gap using the air gap element is four times the number of harmonics. The rotation of the deformed mesh is defined by

$$\begin{bmatrix} x_{rotor} \\ y_{rotor} \end{bmatrix} = \begin{bmatrix} cos(\omega t) & -sin(\omega t) \\ sin(\omega t) & cos(\omega t) \end{bmatrix} . \begin{bmatrix} x_{stator} \\ y_{stator} \end{bmatrix} \tag{15}$$

The generated voltage is computed as a line integral of the electric field, E along the winding. The winding sections are not linked with the two dimensional geometry, hence a proper line integral cannot be carried out. A basic estimation is to disregard the voltage commitments from the ends of the rotor where the winding section is tied. A potential difference is then calculated by taking average z component of the E field for each winding cross-section, multiplying it by the pivot length of the rotor, and taking the aggregate over all winding cross sections.

$$V_i = NN \sum_{winding} \frac{L}{A} \int E_z dA \tag{16}$$

3.h-Hierarchical Adaptivity

Highly complex surfaces are described by hybrid meshes. Hybrid meshes combine the best of regular and irregular meshes as shown in Fig. 3. Irregular meshes have no constraint on the valence of vertices, whereas regular meshes are created by starting from an enormously coarse, uneven base domain and performing recursive refinement, consequential in wide regular grid patches. Both come with different merits and demerits. The regular meshes have very limited flexibility as compared to irregular meshes. The resulting combination of both hybrid meshes is more flexible. Irregular meshes lead to expensive connected data structures and difficult algorithms to refining processes such as smoothening, editing, etc. On the other side regular meshes are regular proficient array based algorithms and data structures which could be easily smoothened or edited. Regular meshes due to their regular shape are compressible. Hybrid meshes also inherit the property of high compressibility.

For the refinement of the mesh a variety of practices are applied out of which h-refinement is mostly preferred. h-refinement is the practice in which two similar dimensional elements are used, but size is changed according to requirement. At some location's size is enlarged and in others reduced in size to provide the minimum cost in approaching the preferred solution. Refinement can easily be implemented and if the presented element shows more error, they are simply

subdivided into smaller elements maintaining the unique undamaged element boundaries. Table 3 shows various mesh statics at different air gaps.

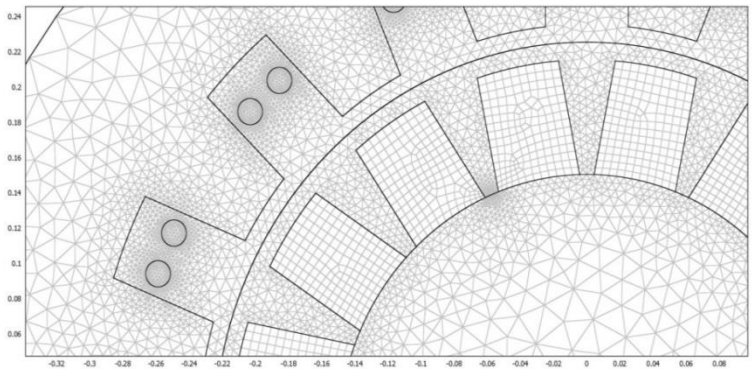

Fig. 3. Reduced model view with mixed mesh.

Table 3. Mesh statics.

Particulars	10 mm	15 mm	20 mm	25 mm	30 mm
Number of degrees of freedom	94203	86161	80953	79553	79871
Number of mesh points	23338	21388	20118	19786	19878
Number of triangular elements	45820	42162	39750	39158	39392
Number of boundary elements	3470	3032	2784	2660	2610
Number of vertex elements	276	276	276	276	276
Minimum element quality	0.667	0.648	0.6906	0.681	0.679
Element area ratio	0.001	0.001	0.0011	0.001	0.001
Number of layers in air gap	4	4	4	4	4
Number of elements in each layer	766	542	396	320	270
Number of unknowns in air gap	3064	2168	1584	1280	1080

4. Results and Discussion

The generated voltage curve was obtained using COMSOL Multiphysics by varying the air gap and magnet material between stator and rotor using the quasi static analysis time dependent solver type. The time stepping at times linearly spaced between 0 to 0.1 with 50 intervals and relative tolerance as $1e^{-2}$. Magnetic flux density is plotted as surface and contour plot as magnetic field in Figs. 4 and 5 respectively.

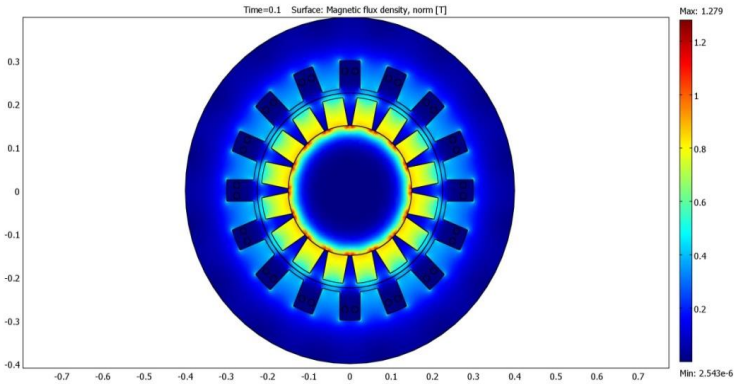

Fig. 4. Surface magnetic flux density.

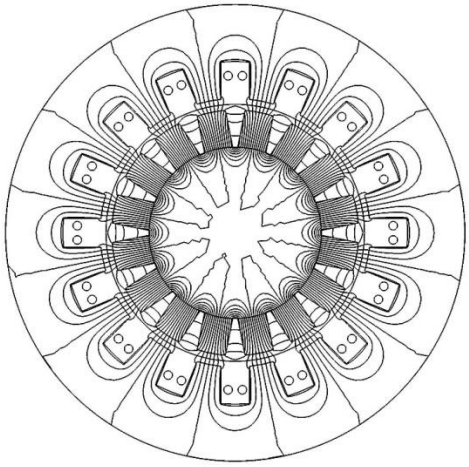

Fig. 5. Contour plot for magnetic potential (A_z).

4.1. Impact of air gap on generated voltage

A permanent magnet machine permits to hold a larger air gap between stator and rotor. The operation of the machine is examined by varying the air gap from 10 mm to 30 mm.

The radial air gap is the touchstone for analyzing the performance of machine as the higher air gap causes a potentially greater impact on the operation of the machine such as cogging, and ripple in the air gap flux density, as well as simplifying machine assembly and lowering initial cost, but the increased air gap offers high resistance to the magnetic flux which adds the magnetizing current and associated losses.

Figure 6 shows magnetic flux density at different air gaps. Figures 7 and 8 present the radial component and tangential component of air gap flux density over one pole pitch, i.e., 45° for 20 mm air gap indicating two cycles of sinusoidal waveform.

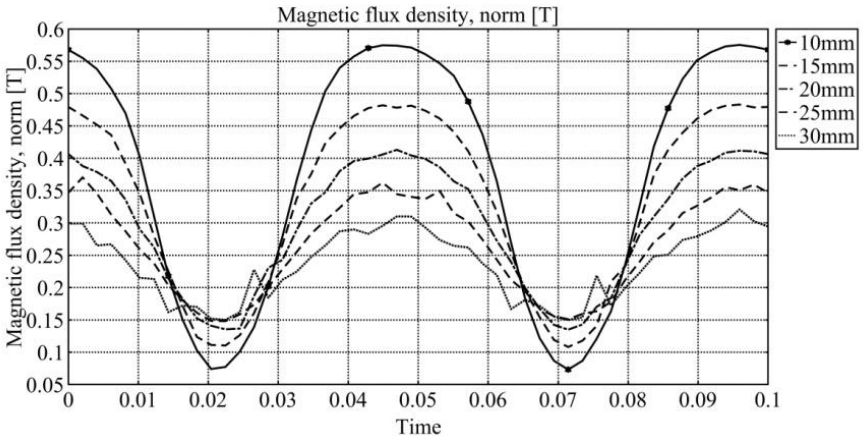

Fig. 6. Magnetic flux density at different air gap using SmCo magnet.

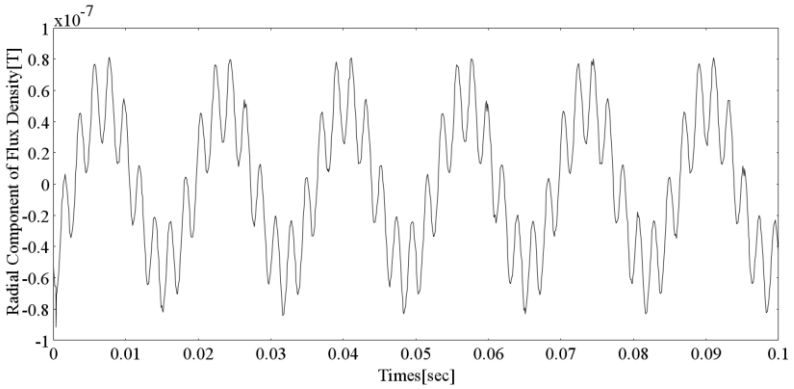

Fig. 7. Radial component of air gap flux density for 20 mm using SmCo24 magnets.

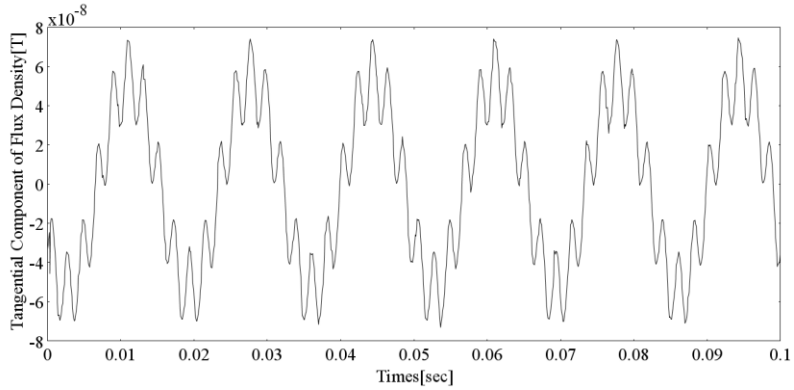

Fig. 8. Tangential component of air gap flux density for 20 mm using SmCo24 magnets.

Generated voltage is plotted with respect to time in Fig. 9. It is observed by reducing the air gap, the voltage generated is increased, but the fact which needs to be considered remains that as the air gap reduces the temperature also increases, which results in poor performance of permanent magnets as they exhibit very poor temperature characteristics.

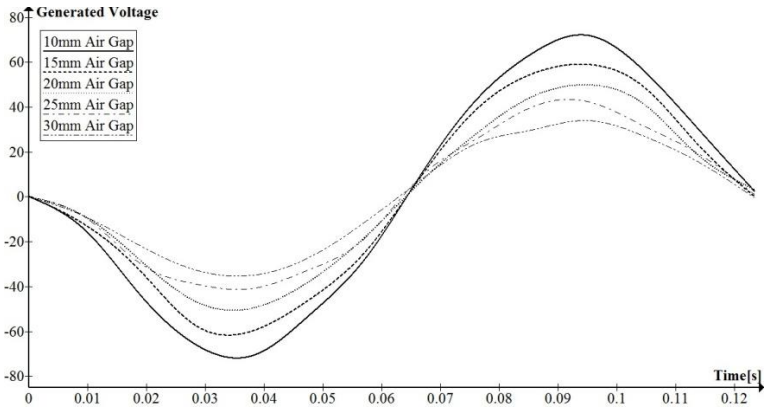

Fig. 9. Generated voltage at different air gaps using SmCo magnets at 60 rpm

4.2. Impact of magnet material on generated voltage

The study of the model at 20 mm air gap was carried out taking into consideration different magnet materials. The generated voltage was plotted as shown in Fig. 10. Alnico was considered in the earliest high-energy magnet to be developed. Attractive features were separated along the residual magnetic field density and coercive force. Alnico has moderately high residual flux density and low coercive force. While ceramic magnets have relatively low residual flux density and high coercive forces, ceramic magnets can endure armature reaction with no demagnetization, but were not favored due to poor mechanical and operational attributes.

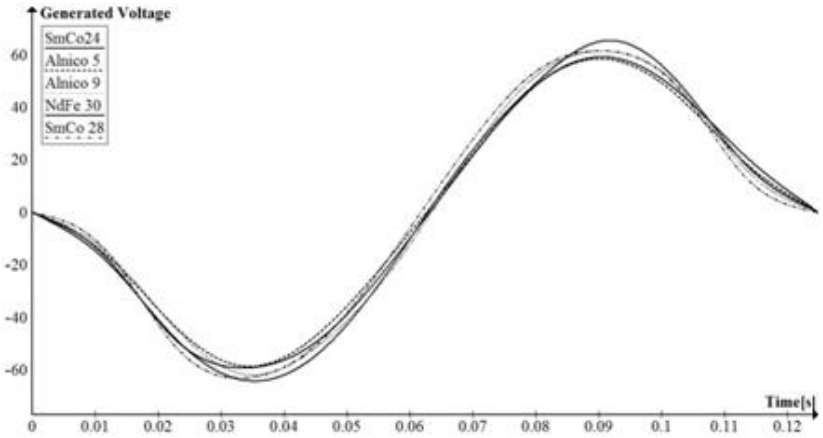

Fig. 10. Generated voltage with different magnet materials.

Samarium-cobalt magnets have a low residual flux density comparable to Alnicos and coercive forces 3-5 times of ceramic magnets and have good mechanical and structural characteristics. NdFe offers the maximum guarantee with enhanced mechanical and structural characteristics and has a relatively low cost compared to Samarium-Cobalt. NdFe has the highest coercive force and relative flux density is highly analogous to Alnicos. The only limitation is they require a low operating temperature. Considering the factor that NdFe has deprived temperature characteristic, it cannot be an alternative to machine applications, so, the property of reduced size and weight is lost. Samarium cobalt is an ideal choice to be considered for rotating machine applications

4.3. Cogging Torque

The cogging torque is developed by the vacillation of the tangential component of the interaction force [22]. An Era component of cogging torque is due to the communication between the rotor magnetic field and the angular variations of the stator reluctance. At the point when the stator and rotor are in relative movement, the attractive conductance which lies between the permanent magnet and the armature. Be that as it may, the attractive conductance changes significantly inside a region which is made out of maybe a couple armature teeth compared with the two side parts of permanent magnet, which can prompt the progressions of the stored energy of the attractive field and after that produce the cogging. Typically cogging torque is dictated by ascertaining the change of the total stored

magnetic energy all around the air gap as to the rotor position and can be communicated as

$$T_C = \frac{dW_{mag}}{d\propto} \tag{17}$$

The waveform of the cogging torque evaluated for the permanent magnet generator is presented in Fig. 11. Cogging torque minimization for PM machines include magnet pole shape, skewing stator tooth or rotor magnets, magnet or pole shifting, pole-arc ratio and stator slot design, dummy slots on the stator teeth, varying the radial shoe depth and graded air gaps [23]. Therefore the authors of this paper decided to integrate some of these techniques in future work for minimization of cogging torque.

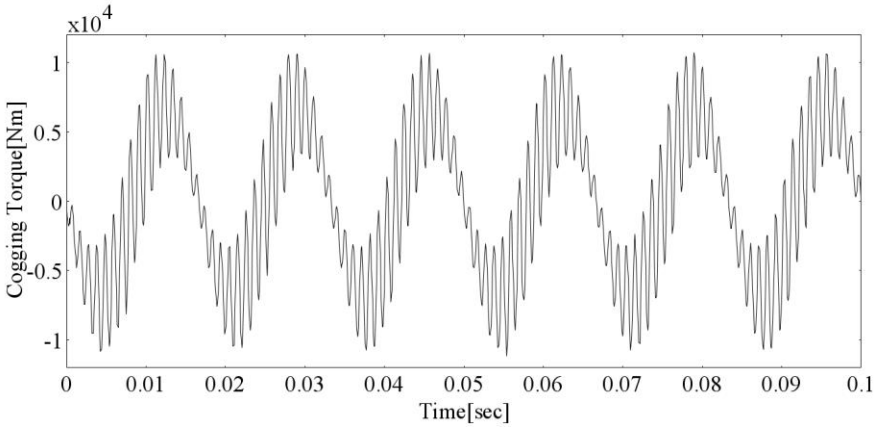

Fig. 11. Cogging torque at 20 mm air gap for SmCo24 magnets

5. Conclusions

A close examination has been made of the impact of the variation of magnetic material and air gap. It has been recorded on a particular form of PM generator and has been broken down to show promise of significant application in the future. This is done using h-hierarchical finite element method using COMSOL Multiphysics. Observations derived from the investigation are as given below.

- The 20 mm air gap is the best optimum air gap for higher generated voltage considering proper mechanical clearance and cooling of the machine.
- Samarium-cobalt magnetic material is considered to be for stable operation of rotating machine applications considering the temperature rise in the machine and is comparatively cost effective and offers higher output on the same frame.

References

1. Kumar, A.; Marwaha, S.; Singh, A.; and Marwaha, A. (2010). Comparative leakage field analysis of electromagnetic devices using finite element and fuzzy methods. *Expert Systems with Applications*, 37(5), 3827-3834.
2. Howey, D.A.; Childs, P.R.N.; and Holmes, A.S. (2012). Air-Gap Convection in Rotating Electrical Machines. *IEEE Transactions on Industrial Electronics*, 59(3), 1367-1375.

3. Polinder, H.; and Hoeijmakers, M.J. (1997). Analytic calculation of the magnetic field in PM machines. *IEEE Industry Applications Conference Thirty-Second IAS Annual Meeting*, 35-41.
4. Watterson, P.A. (2000). Energy calculation of a permanent magnet system by surface and flux integrals (the flux-mmf method). *IEEE Transactions on Magnetics*, 36(2), 470-475.
5. Razek, A.; Maday, Y.; Buffa, A.; Santandrea, L.; Bouillault, E.; and Rapetti, F. (2000). Calculation of eddy currents with edge elements on non-matching grids in moving structures. *IEEE Transactions on Magnetics*, 36(4), 1351-1355.
6. Ciric, I.R. (2000). New model for the computation of quasi-stationary fields due to arbitrary distributions of magnetic dipoles. *IEEE Transactions on Magnetics*, 36(4), 1990-1995.
7. Kim, U.; and Lieu, D.K. (2005). Effects of magnetically induced vibration force in brushless permanent-magnet motors. *IEEE Transactions on Magnetics*, 41(6), 2164-2172.
8. Vicente, P.; Rodríguez, J.; Belahcen, A.; Arkkio, A.; and Laiho, A. (2008). Air-gap force distribution and vibration pattern of Induction motors under dynamic eccentricity, *Electrical Engineering (Archiv fur Elektrotechnik)* , 90(3), 209-218.
9. Belmans, R.; Vandenput, A.; and Geysen, W. (1987). Influence of unbalanced magnetic pull on the radial stability of flexible-shaft induction machines. *IEE Proceedings B.* (*Electric Power Applications*), 134(2), 101-109.
10. Guo, D.; Chu, F.; and Chen, D. (2002). The unbalanced magnetic pull and its effects on vibration in a three-phase generator with eccentric rotor. *Journal of Sound and Vibration*, 254(2), 297-312.
11. Valavi, M.; Matveev, A.; Nysveen, A.; and Nilssen, R. (2014). Multiple-airgap iron-cored direct-driven permanent magnet wind generators, *IEEE International Conference on Electrical Machines (ICEM)*, 578-584.
12. Lai, L.L.; and Chan, T.F. (2007). *Distributed generation: Induction and permanent magnet generators.* UK: John Wiley & Sons, Ltd.
13. Mihai, A.M.; Benelghali, S.; Livadaru, L.; Simion, A.; and Outbib, R. (2012). FEM analysis upon significance of different permanent magnet types used in a five-phase pm generator for gearless small-scale wind. *IEEE XXth International Conference on. Electrical Machines (ICEM)*, 267-273.
14. Andreea, A.; Alecsandru, S.; and Leonard, L. (2014). influence of rotor design over the back emf of permanent magnet synchronous generators. *IEEE International Conference and Exposition on Electrical and Power Engineering (EPE)*, 16-18.
15. Nasar, S.A. (1995). *Electric Machines and Power Systems: Electric machines*. McGraw-Hill.
16. Chen, J.; Nayar, C.V.; and Xu, L. (2000). Design and finite-element analysis of an outer-rotor permanent-magnet generator for directly coupled wind turbines. *IEEE Transactions on Magnetics*, 36(5), 3802-3809.
17. Binns, K.J.; and Wong, T.M. (1984). Analysis and performance of a high-field permanent-magnet synchronous machine. *IEE Proceedings B(Electric Power Applications)*, 131(6), 252-258.

18. Gieras, J.F. (2011). *Permanent magnet motor technology: Design and application* (3rd ed.). CRC Press.
19. Moskowitz, L.R. (1995). *Permanent magnet design and application handbook*. Krieger.
20. Gartner, J. (1999). Improvement of electrical field analysis by use of Computer Aided Software Engineering (CASE) tools. *11th International Symposium on High-Voltage Engineering (ISH 99)*, 132-135.
21. Sroka, J. (1990). On the coupling of the generalized multipole technique with the finite element method. *IEEE Trans. Magnetics*, 26(2), 658-661.
22. Chen, Q.; Shu, H.; and Chen, L. (2012). Simulation analysis of cogging torque of permanent magnet synchronous motor for electric vehicle. *Journal of Mechanical Science and Technology*, 26(12), 4065-4072.
23. Cvetkovski, G.; and Petkovska, L. (2014). Cogging torque minimisation of PM synchronous motor using genetic algorithm. *International Journal of Applied Electromagnetics and Mechanics*, 46(2), 327-334.